Highly Sensitive Non-Classical Strain Gauge Using Organic Heptazole Thin-Film Transistor Circuit on a Flexible Substrate

*Seung Hee Nam, Pyo Jin Jeon, Sung Wook Min, Young Tack Lee, Eun Young Park, and Seongil Im**

A non-classical organic strain gauge as a voltage signal sensor is reported, using an inverter-type thin-film transistor (TFT) circuit, which is able to sensitively measure a large quantity of elastic strain (up to ≈2.48%), which approaches an almost folding state. Novel heptazole-based organic TFTs are chosen to be incorporated in this gauge circuit; organic solid heptazole has small domain size in general. While large crystal domain-pentacene TFTs seldom show sufficient current variation upon mechanical bending for tensile strain, these heptazole TFTs demonstrate a significant variation for the same strain condition as applied to pentacene devices. In addition, the pentacene channel does not recover to its original electric state after bending but heptazole channels are very elastic and reversible, even after going through serious bending. More interesting is that the heptazole TFTs show only a little variation of signal current under horizontal direction strain, while they make a significant amount of current decrease under vertical direction strain. Utilizing the anisotropic response to the tensile bending strain, an ultrasensitive voltage output strain gauge composed of a horizontally and vertically oriented TFT couple is demonstrated.

1. Introduction

Flexible electronics is an attractive research subject that envisages light-emitting,[1–4] sensing,[5–15] wearable,[11–15] logic,[16–18] and memory[19–21] devices on thin flexible substrates. Whether active layers in the devices are organic or inorganic, strain and stress are generated by bending or folding the flexible substrate in general, changing the properties of the devices.[12,13] The strain-induced property changes are undesirable for the device stability in flexible electronics, however if the changes are reversible or elastic in a large strain range, the channel materials in the device may be very useful because they can be attached on machines, clothes, and even the human body to electrically monitor the strain-and-bending behavior of the substrate. As a device to measure or estimate such stress and strain of substrate materials, the classical strain gauge is well known.[22] But a great deal of effort has also been made with organic,[9,10,24–27] oxide,[1,28–30] and Si-based[31–33] thin-film transistors (TFTs), and strain-sensitive capacitors and resistors,[5–15] aiming at flexible plastic and medical electronics. Among many efforts towards strain measurements, utilizing TFTs is quite promising in respects of two-dimensional array mapping, device size, and integration. So, researchers have used several organic or inorganic TFTs either for electrical switches connecting strain sensors[7–9,12] (large size capacitors or resistors) or for a strain-induced sensor by itself.[23] When any TFTs play as strain or bending-induced sensors by themselves, those are mostly limited to irreversible inelastic bending, except in a few cases, because the strain-induced signals can hardly recover to the original state after the release of bending.[13,21,24,34]

Here, we report on a non-classical organic strain gauge as a voltage signal sensor, for the first time using an inverter-type TFT circuit, which is able to sensitively measure a large quantity of elastic strain (up to ca. 2.48% according to a small bending radius of 0.9–1 mm, which approaches an almost folding state). We chose heptazole-based organic TFTs to be incorporated in this gauge circuit; organic solid heptazole has small domain size in general.[35] While a large crystal domain-pentacene TFTs do not show sufficient current variation upon mechanical bending for tensile strain,[25–27] our heptazole TFTs demonstrate quite a significant variation for the same strain condition as applied to pentacene devices. In addition, the pentacene channel does not recover to its original electric state after bending but heptazole channels are very elastic and reversible even after going through a serious bending test where bending radius is ca. 1 mm. More interesting is that the heptazole TFTs show only a little variation of signal current under horizontal direction strain while they make a significant amount of current decrease under vertical direction strain.[36] Utilizing the anisotropic response to the tensile bending strain, we here demonstrate a ultrasensitive voltage-output strain gauge comprised of horizontally and vertically oriented heptazole TFTs

S. H. Nam, P. J. Jeon, S. W. Min, Y. T. Lee, E. Y. Park, Prof. S. Im
Institute of Physics and Applied Physics
Yonsei University
50 Yonsei-ro, Seodaemun-gu
Seoul 120–749, Korea
E-mail: semicon@yonsei.ac.kr

DOI: 10.1002/adfm.201400139

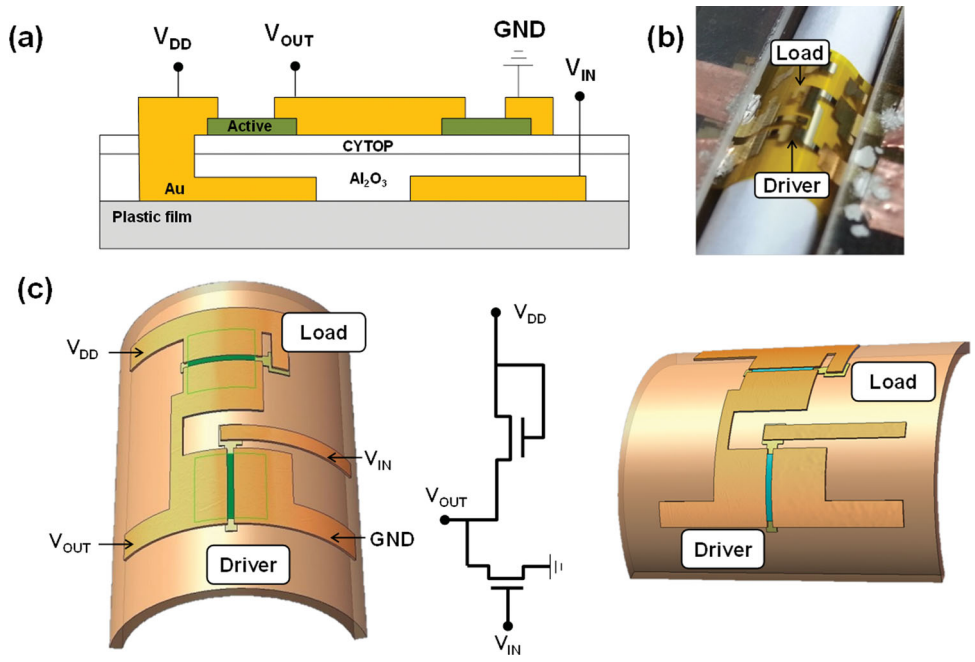

Figure 1. a) Schematic cross-section of our inverter-type strain gauge comprised of two heptazole TFTs. b) Actual image of the strain gauge device as mounted on the bending equipment for tensile stress. c) Circuit diagram and corresponding 3-D schematic view of the strain gauge device, which was integrated with vertically and horizontally oriented heptazole TFTs, respectively, for driver and load on 50 μm thick polyimide substrate. We attempted two types of tensile bending on the gauge, so that driver may get vertical tensile strain while load gets horizontal tensile (left figure), and vice versa (right figure).

that are coupled each other to be an inverter-type device, which could sense the real-time motion of wrist and muscle when attached to a human arm.

2. Results and Discussion

Figure 1a presents a schematic cross-section of our inverter-type device comprising two coupled TFTs (for driver and load), which had a double-layer dielectric (as 20 nm thin organic CYTOP/50 nm thick atomic layer deposited (ALD) Al_2O_3) and patterned Au gate (bottom electrode) on 50 μm thick plastic (polyimide) while their channel width-to-length (W/L) ratios were 500:50 μm. The heptazole active channel layer was deposited on CYTOP, so as to keep the organic channel/organic dielectric interface.[35] Figure 1c displays the circuit (middle) and layouts of our strain gauge device in two types (left: vertical and right: horizontal) of bending for tensile stress, which is shown in actual scheme by a photograph of Figure 1b. The TFT device performance measurements in such bending states were performed with equipment developed to our own design. More details on device fabrication and the bending test are found in the Experimental Section.

Figure 2a shows the drain current–gate voltage (I_D–V_G) transfer characteristics which were achieved at a drain voltage (V_D = –10 V) under many static bending conditions for vertical direction; the static bending states were in the range from 0 to 2.48% (minimum bending radius of ca. 0.9 mm) for tensile strain. The tensile (or compressive) strain vs. bending radius was calibrated and plotted in Figure S1a and S1b (see the Supporting Information (SI)).[13,24,27] According to the transfer curves, tensile strain in static bending clearly reduces I_D (or increases channel resistance), and in fact such decreased I_D value completely recovered after the full release of the bending state (note the curve from the released state; this means that our device properties are elastic and reversible within the strain range; we also observed such elastic behavior in respect of dynamic I_D change, as shown in Figure S2, SI). In contrast to the vertical bending, horizontal direction bending for the same tensile strains never shows any I_D change, as seen in Figure 2b. It is also interesting to know that the other way of bending to cause a compressive strain does make only a little I_D change even in vertical direction bending, unlike the case of tensile strain-generating bending which has made an order-of-magnitude reduction of I_D. Figure 2c displays the transfer curves achieved by vertical compressive strain. As indicated by the inset zoomed view, compressive strain causes a little bit of I_D increase (dotted curves indicate buckling failure over –2.3% compressive strain). Compressive strain in horizontal direction bending appeared to provide no effects to the TFT, as expected (Figure 2d).

Similar strain effects were observed from organic pentacene-channel TFTs fabricated on the same dielectric, except for one critical problem whereby the bending induces a plastic deformation of the channel with no full elastic recovery (see the inset of Figure 2e); another difference is that, according to the transfer curves of Figure 2e, the strain-induced I_D decrease is shown to be relatively smaller than that of heptazole TFTs. Again, compressive strain in horizontal direction bending has no effect on the pentacene TFT (Figure 2f). Why only the vertical way of tensile bending significantly affects the device is a first and primary question to be answered. According to

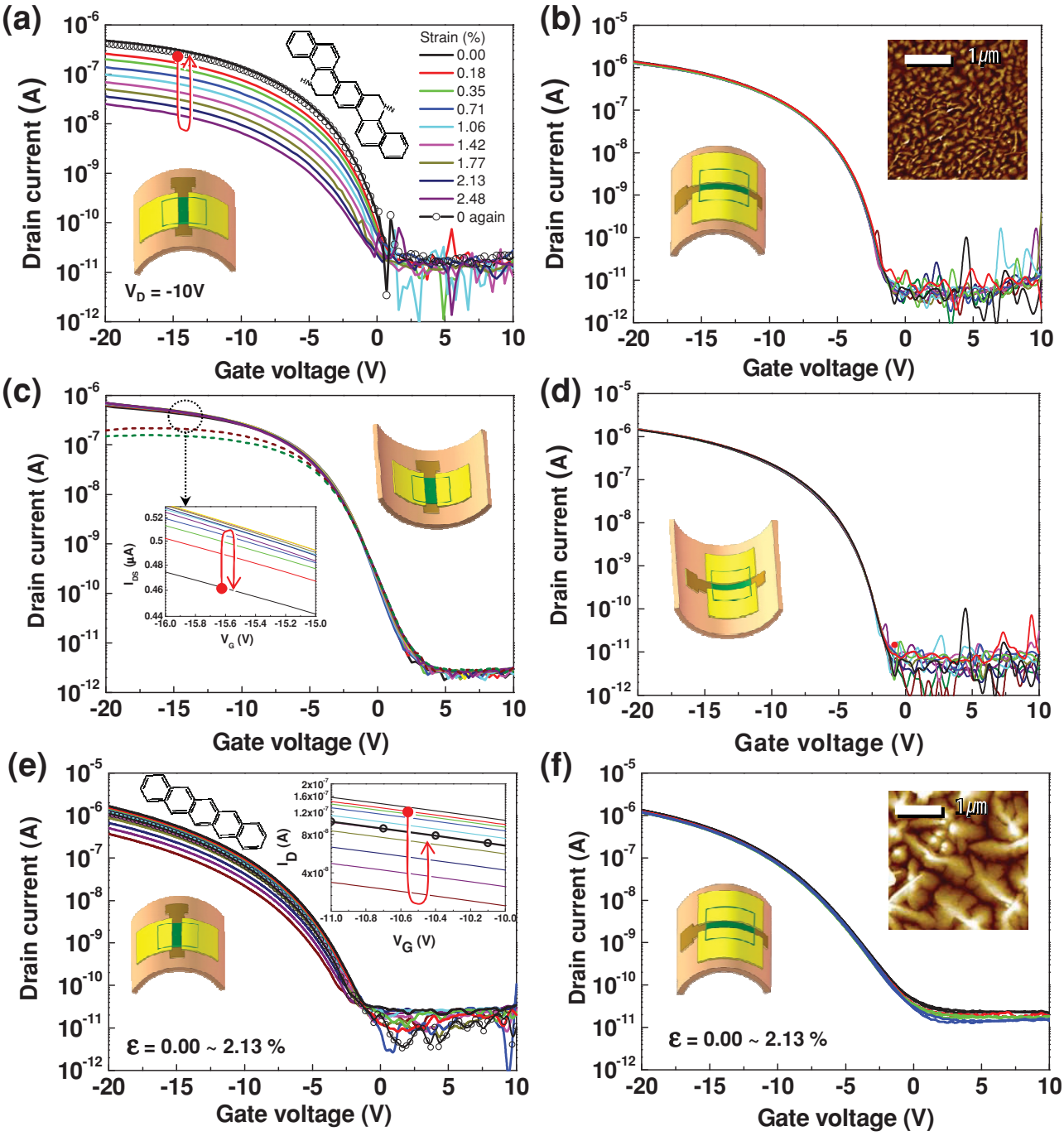

Figure 2. The drain current–gate voltage (I_D–V_G) transfer curves achieved from heptazole TFTs at a drain voltage (V_D = –10 V) under static bending conditions in the range from 0% to 2.48%: a) vertical tensile strain bending, b) horizontal tensile strain bending, c) vertical compressive strain bending, and d) horizontal compressive strain bending. Transfer curves from pentacene TFTs at a drain voltage (V_D = –10 V) under static bending conditions in the range from 0% to 2.13%: e) vertical tensile strain bending, and, f) horizontal tensile strain bending. The insets in Figure 2b and 2f are the atomic force microscope (AFM) images displaying heptazole and pentacene channel surfaces in our TFTs, respectively.

previous reports on inorganic TFTs, the serious tensile bending toward vertical direction seems to cause microcrack lines that form in a vertical direction to source-to-drain (S-D) direction, while the same bending toward horizontal direction forms another microcracks in a parallel direction.[23,26,27] If the tensile bending is small enough to conserve the elastic recovery behavior of organic TFT channel, such microcracks are too premature to allow any plastic deformation, but the free carriers in organic heptazole channel might still face premature microcracks or increased intergranular spacings as hopping barriers against hole transport from S to D electrode (we suspect that the grain boundary spacing may increase under the

elastic tensile strain). The hopping barriers should increase the channel resistance and decrease I_D.[23,26,27] On the contrary, the strain-induced intergranular spacings in parallel (horizontal) orientation to S–D would not decrease I_D since the free hole-carriers can be still straightforwardly transported from S to D without any effective barriers in this case. Since the heptazole channel is comprised of much smaller grains (50–100 nm size in atomic force microscopy images, see Figure 2b inset) than that (Figure 2f inset) of solid pentacene, it should have a much larger number of grain boundaries[35] which act as the hopping barrier of hole carriers. It is classically acceptable that materials with many isotropic small grains are more elastically deformable than the others with a few large grains,[37] so now we consider that small grain size of heptazole could be one possible origin for the observed elastic bending behavior. Although the heptazole channel TFT has a smaller mobility (or smaller ON current) than that of pentacene TFT in general, it would more stably and sensitively operate as a component of elastic strain gauge with the benefits of much higher numbers in channel grain boundaries. We investigated another type of organic TFT (with the same CYTOP/Al_2O_3 dielectric) which has n-channel PTCDI-C13, to support the grain size effects on the elastic deformation behavior because the 50 nm thick PTCDI-C13 shows a large domain size in general. According to the transfer curves of Figure S3 (see the SI), vertically strained PTCDI-C13 TFT hardly shows any elastic reversible I_D behavior unlike the heptazole TFT, but presents almost plastic deformation behavior which is even worse than that of pentacene TFT in reversibility aspects. The PTCDI-C13 channel film not only shows its large grains (as large as 0.5–1 μm) but also terrace-structured domains which may come from the packing efficiency of PTCDI-C13 molecules. Since the elastic heptazole and partially-elastic pentacene films basically show herringbone-structured surface morphologies, it is regarded that smaller grain organics with herringbone structure may have an advantage in elastic behavior.

Figure 3a shows the voltage transfer curves (VTCs) obtained from our organic strain gauge under tensile strain bending; the inset illustrates the bent inverter-type organic device utilizing aforementioned two TFTs as load and driver. According to the inset illustration, the load TFT is bent horizontally but the driver is vertically bent, which means that the load would have a fixed channel resistance while the driver would display strain-dependent resistance. Hence, the VTC curves now show their output voltage (V_{OUT}) signals as a function of not only the input voltage (V_{IN}) but also the elastic tensile strain by bending. Applied supply voltage (V_{DD}) was −10 V in the circuit and we chose V_{IN} of −10 V to observe V_{OUT} which would dynamically decrease in time domain depending on the mechanical elastic strain (ε, %) by tensile bending. As a result, we achieved the strain-induced dynamic V_{OUT} curves that also display their elastic recoveries in Figure 3b. The elastic bending for tensile strain appeared to provide the decrease of V_{OUT} in time domain and in the range of 0–2.48% without any mechanical failure or plastic deformation (here, we show the behavior by 0.71%). Similar strain-induced V_{OUT} behavior was observed by the same inverter but under different direction of tensile strain bending (Figure 3c): according to the inset illustration of Figure 3c, the load TFT is vertically but the driver is horizontally bent, which means that the driver would have a fixed channel resistance while the load would display strain-dependent resistance. Applied supply voltage (V_{DD}) was again −10 V in the circuit and this time we chose V_{IN} of −5 V to observe V_{OUT}, which would dynamically increase in time domain depending on the elastic strain (ε, %) by tensile bending, which was elastically reversible upto 2.13% in respect of V_{OUT}, as shown in Figure 3d (here, we show the behavior at 1.42%). It is worthy of note that in Figure 3c V_{OUT} increases (becomes less negative) with tensile strain, unlike the other case of Figure 3a due to the different bending configuration. Also, see that the inset photo of Figure 3c shows 2.3% strain-induced bending which leads to ca. 1 mm radius, an almost-folding state of our 50 μm thick plastic substrate. A pentacene TFT-based strain gauge inverter appeared also operational as shown in another VTC curves of Figure 3e, however, it showed some of plastic deformation behavior, too (see the inset). Since the pentacene-based system was not very elastic and its recovery behavior was a little slow after release of bending, its time-domain V_{OUT} behavior appeared quite undesirable in Figure 3f, where the signs of plastic deformation of pentacene TFT become more obvious with the tensile strain. It is now highly regarded that the heptazole channel for conserving the elasticity is much advantageous over pentacene channel, and the reason may come from their different crystal domain sizes and grain boundary numbers as discussed in Figure 2a and f.

On the one hand, our organic heptazole strain gauge under compressive strain-generating bending was found not to work so well as under tensile strain bending according to Figure S4 (see the SI), where a large compressive bending strain of more than ≈ −2.4% is necessary to obtain a small amount of elastic strain-induced ΔV_{OUT} (0.2 V increase), which is consistent with the results from compressive strain-induced I_D in Figure 2c. We also found a plastic deformation (or failure) at −2.66% along with V_{OUT} decrease (see Figure S4, SI). The compressive bending does not make any significant output signals in I_D and V_{OUT} because it hardly causes any increased intergranular barrier in heptazole organic channel but ooes serious buckling damage to the material in the end. However, it may decrease the channel length as the compressive strain gets large. Equation (1) describes I_D behavior in current saturation of a TFT:[10,23]

$$I_D = \frac{1}{2}\mu C_{OX}\frac{W}{L}(V_G - V_{TH})^2 \quad (1)$$

where μ is the saturation mobility, C_{OX} is constant as a dielectric capacitance per unit area, W/L is the width to length ratio of channel, and V_{TH} is threshold voltage of the TFT. The saturation mobility, μ would be almost constant except the case of tensile bending toward vertical direction, which forms the gap widening of grain boundaries against charge transport decreasing μ and I_D as we discussed in Figure 2a. The reduced channel length, ($L - \Delta L$) which is obtained by compressive bending may mechanically cause ($W + \Delta W$), resulting in an increased I_D in vertical compressive strain bending case according to the above Equation (1) (more details on the strain-induced W/L geometry versus I_D are introduced in Figure S5 in the SI). So, a significant compressive strain makes only a little change (increase) of I_D and V_{OUT} which is incomparably smaller than that from the same amount of tensile strain, which would

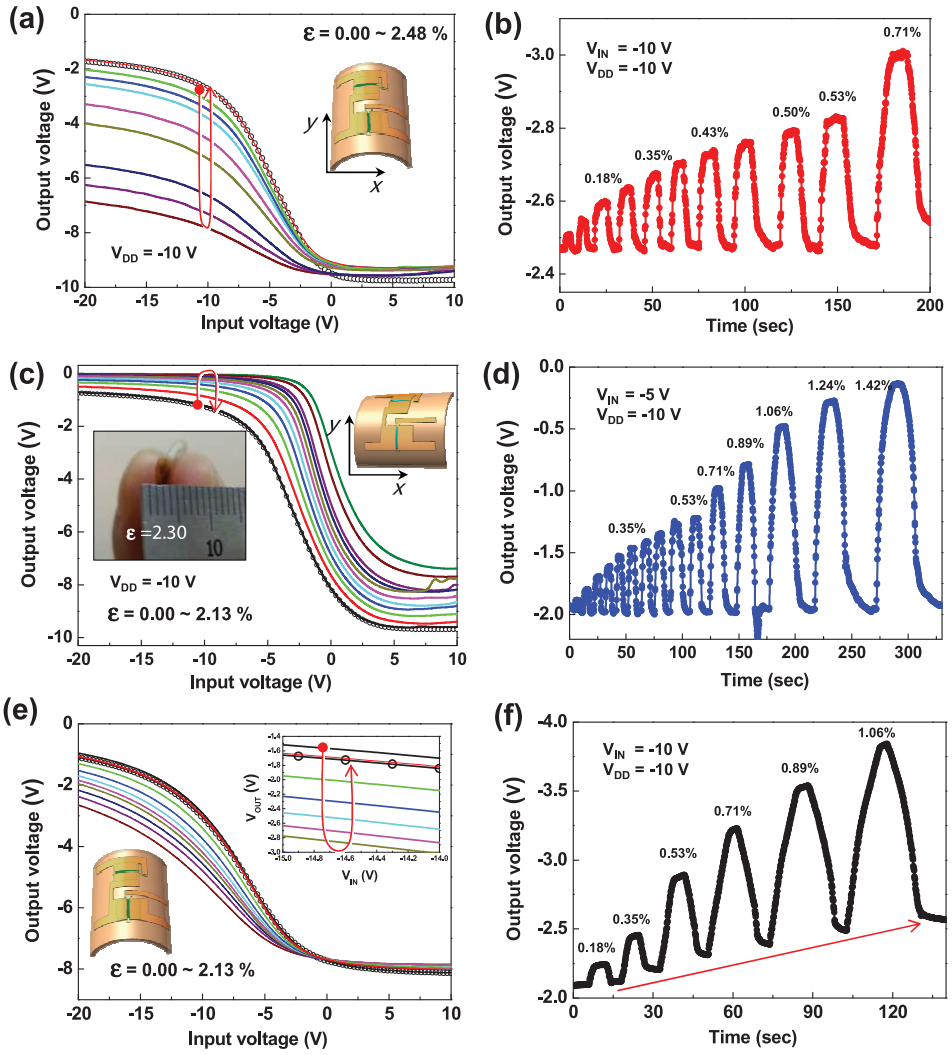

Figure 3. Voltage transfer characteristics (VTCs) of our inverter-type heptazole-based strain gauge, as obtained by sweeping input voltage from V_{IN} = −20 V to 10 V: a) vertical strain bending on driver TFT but horizontal bending on load as shown in the inset, which leads to the output voltage dynamics of: b), and, c) vertical strain bending on load TFT but horizontal bending on driver as shown in the inset, which leads to the output voltage dynamics of d). The inset photo of Figure 3c shows 2.3% strain-induced bending which leads to ca. 1 mm radius, almost a folding state of our 50 μm-thick plastic substrate. VTC behavior of the pentacene-based strain gauge inverter as obtained from the same sweeping conditions: e) vertical strain bending on driver TFT but horizontal bending on load as shown in the inset, which leads to the output voltage dynamics of f). Some evidence of plastic deformation is indicated by the arrow; with more strain more inelastic behavior appears along with quite a slow dynamics.

change the channel mobility. This indicates that the presence of the intergranular hopping barriers is important for the effective functioning of our organic strain gauge, while expecting V_{OUT} signal change by W/L dimension variation is not very practical. Both results from elastic tensile and compressive bending on the organic strain gauge are summarized in more detailed manner in Figure S6, where strain versus ΔV_{OUT} relation is plotted for any convenience toward strain gauge applications and gauge factor (GF) calculations. GF is calculated as a slope of the $\Delta V_{OUT}/V_o$ versus ε plot in our case which has a supply current (I_{DD}) in a simple series connection of two TFTs for an inverter and V_o is an initial V_{OUT} (flat state without strain). GF values were respectively worked out to be 0.86 and 0.043 for tensile and compressive bending, which are quite comparable to those from recent reports.[12,38]

Figure 4a,d demonstrate the performance of our heptazole-based strain gauge device as attached on the wrist joint and muscle of a human arm (the inset of Figure 4a displays a magnified photo of the strain gauge inverter attached on the wrist). When straining and releasing are repeated, our strain gauge well operates in both respects of sensitivity (ΔV_{OUT}) and reaction speed. Figure 4b shows the large output signals obtained from wrist joint motion. In particular, the muscle motion (see photos in Figure 4c) was quite sensitively recorded as shown in Figure 4d and in a short video in the SI (strain gauge.avi). According to Figure 4d, a small output (ΔV_{OUT}) of 0.03 V is continuously reproduced from repetitive muscle straining, which is estimated to be ca. 0.04% from the output dynamics in Figure 3b. Based on such demonstrations, we positively regard that our ultrasensitive organic strain gauge may be useful for

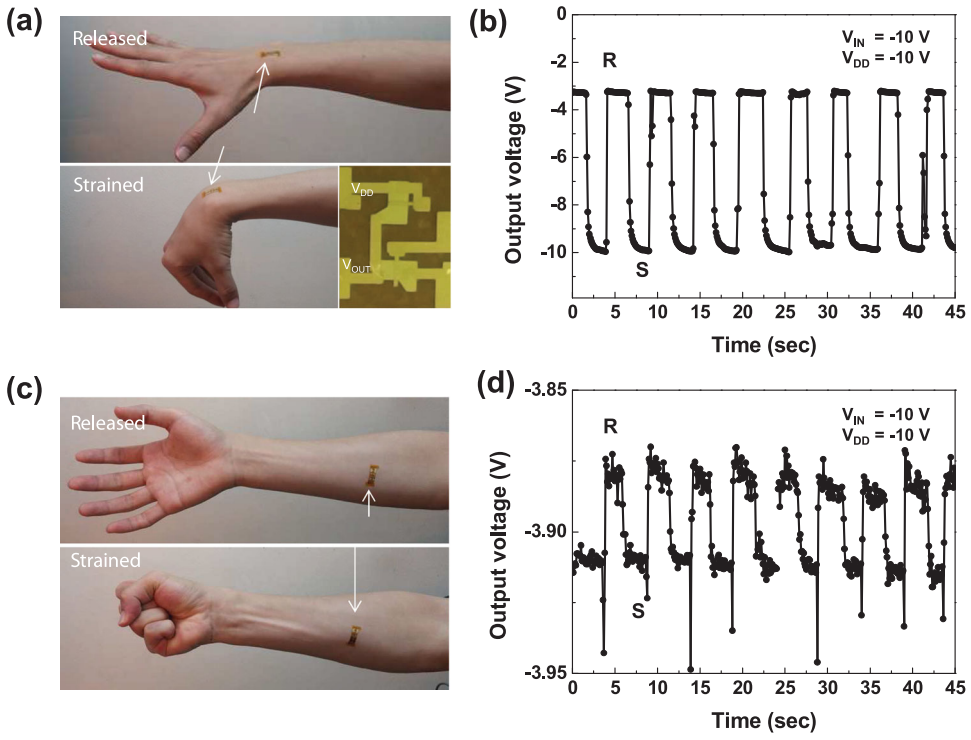

Figure 4. a) Photographs of our strain gauge inverter attached on the wrist as released and strained states (the inset shows the optical microscopy image of our device). b) The dynamic voltage response reflects the motion of wrist joint (R: released state, S: strained state). c) Photographs of our strain gauges on a fore arm, and, d) contraction and relaxation of the muscle was sensitively detected by the same device. About 0.04% strain is estimated from this muscle motion (by ca. 0.03 V output variation).

wearable/flexible and even human medical applications in the future.

3. Conclusion

In summary, we have fabricated an inverter-type organic strain gauge to measure a quantitative strain amount upon bending radius, utilizing heptazole-based TFTs. Our heptazole TFT-based strain gauge demonstrates quite a significant output signal voltage as constructed with a pair of TFTs where one organic TFT shows insignificant I_D under tensile strain by horizontal direction bending while the other makes a considerable amount of I_D decrease under the same tensile strain but by vertical direction bending. The main difference of I_D is attributed to the anisotropic widening of intergranular gap under tensile bending. Utilizing such anisotropic response to the tensile bending strain, we for the first time demonstrated a non-classical strain gauge to sensitively detect the motions of muscle and joint of human arm. We conclude that our organic gauge is practically promising for the strain-sensing applications in future flexible/wearable electronics.

4. Experimental Section

Device Fabrication: The organic strain gauge device is a low-voltage gain enhancement mode inverter with two heptazole-based bottom-gate TFTs[35] on a flexible film. A bottom gate electrode of 50 nm thick Au was thermally evaporated and patterned through a shadow mask on the 50 μm thick polyimide film, which was attached on a glass supporter. A 50 nm thick Al_2O_3 was then deposited on the gate using atomic layer deposition system (ALD) at 100 °C as a gate dielectric insulator, followed by a 20 nm thin CYTOP that was spin-coated and thermally cured at 180 °C for 120 min. The CYTOP would nicely match with organic small molecule heptazole layer at the interface, when the 50 nm thick heptazole was thermally deposited through a shadow mask as an active channel layer by organic molecular beam deposition system at a deposition rate of 0.1 nm s^{-1} and at room temperature. Then, a 50 nm thick Au was thermally evaporated and patterned as a source/drain and interconnection. The driver and load TFTs were positioned at the center of the substrate to ensure the same strain on both as shown in Figure 1b and 1c. The W/L ratio of our organic TFTs was 500:50 μm.

Bending Test Setup and Measurement: The flexible plastic substrate film with the inverter-type strain gauge was mounted on a bending mechanism, which has two mobile grips to hold two sides of our gauge and is simultaneously able to change the interval between the two sides. The substrate film was initially flat, which is for 0% strain, and with an initial 10 mm interval between two grips. When the bending strain measurement started, the interval was mechanically reduced by a micro-positioner. The Bending radius, R, was calibrated with the interval, since they are in a certain relationship as shown in Figure S1a–d (see the SI). The input and output terminals of our organic strain gauge were connected to semiconductor parameter analyzer (Model HP 4155C, Agilent Technologies) through BNC cables; their terminal electrodes were patterned to be large enough to accept crocodile clips. In this way we measured the bending-dependent electrical properties of our devices in both static and dynamic bending situations whether the device is an organic TFT or the inverter-type organic gauge. Measured R was converted to strain, ε by using Equation 2 (which is also shown in Figure S1, SI):[24,27]

$$\varepsilon = \frac{(d_f + d_s)}{2R} \frac{(1 + 2\eta + \chi\eta^2)}{(1+\eta)(1+\chi\eta)} \quad (2)$$

where $\eta = d_f/d_s$ and $\chi = E_f/E_s$, d_f is the deposited film thickness, d_s is the substrate thickness, and E_f and E_s are the Young's moduli of film and substrate, respectively. The strain, ε appears positive or negative depending on R, which is positive for tensile strain but negative for compressive strain. Here, we simplified the above strain calculation only plugging in Young's modulus and film thickness of Al_2O_3 for E_f and d_f, ignoring those of organic CYTOP and heptazole films, which would be too soft to have any significant modulus.

Supporting Information

Supporting Information is available from the Wiley Online Library or from the author.

Acknowledgements

S.H.N. and P.J.J. have contributed equally to this research. The authors acknowledge the financial support of the NRF (NRL program: Grant No. 2009–0079462), the Ministry of Knowledge Economy in Republic of Korea (Grant No. 10042433–2012–11), and Brain Korea 21 plus.

Received: January 15, 2014
Revised: January 28, 2014
Published online: April 6, 2014

[1] A. Nadarajah, R. C. Word, J. Meiss, R. Könenkamp, *Nano Lett.* **2008**, *8*, 534.
[2] T. Sekitani, H. Nakajima, H. Maeda, T. Fukushima, T. Aida, K. Hata, T. Someya, *Nat. Mater.* **2009**, *8*, 494.
[3] G. Gustafsson, Y. Cao, G. M. Treacy, F. Klavetter, N. Colaneri, A. J. Heeger, *Nature* **1992**, *11*, 477.
[4] A. N. Krasnov, *Appl. Phys. Lett.* **2002**, *80*, 3853.
[5] S. C. B. Mannsfeld, B. C. Tee, R. M. Stoltenberg, C. V. Chen, S. Barman, B. V. Muir, A. N. Sokolov, C. Reese, Z. Bao, *Nat. Mater.* **2010**, *9*, 859.
[6] D. J. Lipomi, M. Vosgueritchian, B. C. Tee, S. L. Hellstrom, J. A. Lee, C. H. Fox, Z. Bao, *Nat. Nanotechnol.* **2011**, *6*, 788.
[7] K. Takei, T. Takahashi, J. C. Ho, H. Ko, A. G. Gillies, P. W. Leu, R. S. Fearing, A. Javey, *Nat. Mater.* **2010**, *9*, 821.
[8] T. Sekitani, T. Yokota, U. Zschieschang, H. Klauk, S. Bauer, K. Takeuchi, M. Takamiya, T. Sakurai, T. Someya, *Science* **2009**, *326*, 1516.
[9] T. Someya, T. Sekitani, S. Iba, Y. Kato, H. Kawaguchi, T. Sakurai, *Proc. Natl. Acad. Sci. U.S.A.* **2004**, *101*, 9966.
[10] T. Someya, A. Dodabalapur, J. Huang, K. C. See, H. E. Katz, *Adv. Mater.* **2010**, *22*, 3799.
[11] T. Yamada, Y. Hayamizu, Y. Yamamoto, Y. Yomogida, A. Izadi-Najafabadi, A. N. Futaba, K. Hata, *Nat. Nanotechnol.* **2011**, *6*, 296.
[12] D. H. Kim, N. Lu, R. Ma, Y. S. Kim, R. H. Kim, S. Wang, J. Wu, S. M. Won, H. Tao, A. Islam, K. J. Yu, T. Kim, R. Chowdhury, M. Ying, L. Xu, M. Li, H. J. Chung, H. Keum, M. McCormick, P. Liu, Y. W. Zhang, F. G. Omenetto, Y. Huang, T. Coleman, J. A. Rogers, *Science* **2011**, *333*, 838.
[13] K. Fukuda, K. Hikichi, T. Sekine, Y. Takeda, T. Minamiki, D. Kumaki, S. Tokito, *Sci. Rep.* **2013**, *3*, 2048.
[14] C. Pang, G. Y. Lee, T. Kim, S. M. Kim, H. N. Kim, S. H. Ahn, K. Y. Suh, *Nat. Mater.* **2012**, *11*, 795.
[15] B. S. Shim, W. Chen, C. Doty, C. Xu, N. A. Kotov, *Nano Lett.* **2008**, *8*, 4151.
[16] U. Zschieschang, T. Yamamoto, K. Takimiya, H. Kuwabara, M. Ikeda, T. Sekitani, T. Someya, H. Klauk, *Adv. Mater.* **2011**, *23*, 654.
[17] T. Sekitani, U. Zschieschang, H. Klauk, T. Someya, *Nat. Mater.* **2010**, *9*, 1015.
[18] U. Zschieschang, F. Ante, T. Yamamoto, K. Takimiya, H. Kuwabara, M. Ikeda, T. Sekitani, T. Someya, K. Kern, H. Klauk, *Adv. Mater.* **2010**, *22*, 982.
[19] S.-J. Kim, J.-S. Lee, *Nano Lett.* **2010**, *10*, 2884.
[20] W. J. Yu, S. H. Chae, S. Y. Lee, D. L. Duong, Y. H. Lee, *Adv. Mater.* **2011**, *23*, 1889.
[21] Y. Ji, B. Cho, S. Song, T.-W. Kim, M. Choe, Y. H. Kahng, T. Lee, *Adv. Mater.* **2010***22*, 3071.
[22] K. Hoffmann, "An Introduction to Measurements using Strain Gages", *Hottinger Baldwin Messtechnik GmbH, Darmstadt* **1989**, 127.
[23] T. Sekitani, Y. Kato, S. Iba, H. Shinaoka, T. Someya, T. Sakurai, S. Takagi, *Appl. Phys. Lett.* **2005**, *86*, 073511.
[24] P. Cosseddu, G. Tiddia, S. Milita, A. Bonfiglio, *Org. Electron.* **2013**, *14*, 206.
[25] P. Cosseddu, S. Milita, A. Bonfiglio, *IEEE Electron Device Lett.* **2012**, *33*, 113.
[26] V. Scenev, P. Cosseddu, A. Bonfiglio, I. Salzmann, N. Severin, M. Oehzelt, N. Koch, J. P. Rabe, *Org. Electron.* **2013**, *14*, 1323.
[27] F.-C. Chen, T.-D. Chen, B.-R. Zeng, Y.-W. Chung, *Semicond. Sci. Technol.* **2011**, *26*, 034005.
[28] K. Nomura, H. Ohta, A. Takagi, T. Kamiya, M. Hirano, H. Hosono, *Nature* **2004**, *432*, 488.
[29] N. Münzenrieder, K. H. Cherenack, G. Tröster, *IEEE Trans. Electron Devices* **2011**, *58*, 2041.
[30] K. H. Cherenack, N. S. Münzenrieder, G. Tröster, *IEEE Electron Device Lett.* **2010**, *31*, 1254.
[31] T. Serikawa, F. Omata, *IEEE Trans. Electron Devices* **2002**, *49*, 820.
[32] T. Afentakis, M. Hatalis, A. T. Voursas, J. Hartzell, *IEEE Trans. Electron Devices* **2006**, *53*, 815.
[33] A. Pecora, L. Maiolo, M. Cuscunà, D. Simeone, A. Minotti, L. Mariucci, G. Fortunato, *Solid-State Electron.* **2008**, *52*, 348.
[34] A. N. Sokolov, Y. Cao, O. B. Johnson, Z. Bao, *Adv. Funct. Mater.* **2012**, *22*, 175–183.
[35] J. H. Park, H. S. Lee, S. Park, S.-W. Min, Y. Yi, C.-G. Cho, J. Han, T. W. Kim, S. Im, *Adv. Funct. Mater.* **2014**, *24*, 1109.
[36] A. Nigam, G. Schwabegger, M. Ullah, R. Ahmed, I. I. Fishchuk, A. Kadashchuk, C. Simbrunner, H. Sitter, M. Premaratne, V. R. Rao, *Appl. Phys. Lett.* **2012**, *101*, 083305.
[37] G. E. Dieter, *Mechanical Metallurgy* McGraw-Hill, D. J. Conroy, NY, USA **1961**, 195.
[38] N. Lu, C. Lu, S. Yang, J. Rogers, *Adv. Funct. Mater.* **2012**, *22*, 4044.